

narrow laminar regime close to the transition from axisymmetric to non-axisymmetric flow, far from the regime of geostrophic turbulence. In the experiments of both Hide and Read and Antipov *et al.* the forcing was axisymmetric, which contrasts with the localized forcing produced by our pumping through inlets and outlets. The small scale of our forcing could be significant because such forcing is generally a necessary condition for strong turbulence in a quasi-two-dimensional flow (energy transfers towards small scales are inhibited).

Our experiment demonstrates that for a wide range of conditions a permanent coherent vortex, like the long-lived coherent spots on Jupiter, can emerge spontaneously from a turbulent, incompressible, quasi-geostrophic flow. It is not necessary to invoke stratification or deformation of the fluid layer to explain the formation of a stable spot. The dynamical behaviour is dominated by two-dimensional inertia and the beta effect; frictional effects are secondary, as on Jupiter.

Our experiments and the simulation of Marcus¹ suggest that long-lived vortices should form in planetary zones of strong shear and uniform potential vorticity. Recent estimates¹⁸ indicate that the potential vorticity is fairly uniform for the zonal flows that contain the Great Red Spot and the White Oval BC, but further measurements are needed for other latitudes where long-lived vortices are located.

We thank Philip Marcus for suggesting this experiment. This research is supported by the NSF Program in Fluid Mechanics and Hydraulics, the Office of Naval Research Nonlinear Dynamics Program, and the Exxon Education Foundation. J.S. is supported in part by the Centre National de la Recherche Scientifique.

Received 16 June, accepted 11 December (1987).

1. Marcus, P. S. *Nature* **331**, 693–696 (1988).
2. Pedlosky, J. *Geophysical Fluid Dynamics* (Springer, New York, 1979).
3. Beebe, R. F. & Hockey, T. A. *Icarus* **67**, 96–105 (1986).
4. MacLow, M. M. & Ingersoll, A. P. *Icarus* **65**, 353–369 (1986).
5. Mitchell, J. L., Beebe, R. F., Ingersoll, A. P. & Garneau, G. W. *J. geophys Res.* **86**, 8751–8757 (1981).
6. Williams, G. P. *Adv. Geophys.* **28A**, 381–427 (1985).
7. Ingersoll, A. P. & Cuong P. G. *J. atmos. Sci.* **38**, 2067–2076 (1981).
8. Hatzes, A., Wenkert, D. D., Ingersoll, A. P. & Danielson, G. E. *J. geophys. Res.* **86**, 8754–8749 (1981).
9. Flasar, F. M. *Icarus* **65**, 280–303 (1986).
10. Colin de Verdier, A. *Geophys. Astrophys. Fluid Dyn.* **15**, 213–251 (1980).
11. McEwan, A. D., Thompson, R. O. R. Y. & Plum, R. A. *J. Fluid Mech.* **9**, 655–672 (1980).
12. Antipov, S. V., Nezlin, M. V., Slezkin, E. N. & Trubnikov, A. S. *Nature* **323**, 238–240 (1986).
13. Read, P. L. & Hide, R. *Nature* **308**, 45–48 (1984).
14. Hide, R. & Titman, C. W. *J. Fluid Mech.* **29**, 39–60 (1967).
15. Rabaud, M. & Couder, Y. *J. Fluid Mech.* **136**, 291–319 (1983).
16. Maxworthy, T. & Redekopp, L. G. *Icarus* **29**, 261–271 (1976).
17. Petviashvili, V. I. *Soviet Astr. Lett.* **9**, 137–138 (1983).
18. Dowling, T. E. & Ingersoll, A. P. *J. atmos. Sci.* **45** (1988).

Numerical simulation of Jupiter's Great Red Spot

Philip S. Marcus

Department of Mechanical Engineering, University of California at Berkeley, Berkeley, California 94720, USA

Jupiter's Great Red Spot is viewed as a vortex that arises naturally from the equations of motion of the jovian atmosphere. Here I solve numerically the equations governing fluid motion in a model of the jovian atmosphere for a variety of initial conditions. Large spots of vorticity form spontaneously in chaotic azimuthal flows and are stable if the vorticity of the spots has the same sign as the shear of the surrounding azimuthal flow. The Great Red Spot is compared with these solutions and a new prediction of its vertical structure is made.

Following Ingersoll and Cuong¹, I use a two-layer model in which the Great Red Spot lies in a shallow layer overlying a

deep azimuthal flow. In this model the shallow upper layer does not influence the denser flow beneath it, but the deep azimuthal flow affects the upper layer by determining its vertical depth. The velocity v of the upper layer is approximated as two-dimensional (due to the rapid rotation of the planet) and is determined by potential vorticity ω_p conservation:

$$\left[\frac{\partial}{\partial t} + (\mathbf{v} \cdot \nabla) \right] \omega_p = \frac{D\omega_p}{Dt} = 0 \quad (1)$$

We use the quasi-geostrophic β -plane approximation² for ω_p of the upper layer:

$$\omega_p(r, \phi, t) = \omega(r, \phi, t) - \beta r - \frac{\psi(r, \phi, t) - \bar{\psi}(r)}{L_R^2} \quad (2)$$

where β is the gradient of the Coriolis force, ϕ is the longitude, r is the latitude of Jupiter multiplied by its radius, $L_R = (\sqrt{gH\Delta\rho/\rho})/f$ is the Rossby deformation radius (a measure of the vertical stratification), f is twice Jupiter's angular velocity, $\Delta\rho$ is the difference in density between the lower and upper layers, and ρ , H , g , $\psi(r, \phi, t)$ and $\omega(r, \phi, t) \equiv \nabla^2\psi(r, \phi, t)$ are the density, mean vertical depth, gravitational acceleration, stream function and vorticity of the upper layer. The azimuthal velocity of the lower layer is given by the stream function $\bar{\psi}(r)$. The physics responsible for the deep flow (convection, latent heat release, radiation and differential heating, for example) occurs on timescales that are much longer^{1,3} (10^8 s) than the dynamical or turn-around time of the spot ($\sim 10^6$ s). (In the five months between the fly-bys of Voyagers 1 and 2, there was no appreciable change in Jupiter's azimuthal zones⁴.) Therefore we treat $\bar{\psi}(r)$ as a time-independent, but unknown, parameter that we vary to obtain different numerical solutions. Here, equations (1) and (2) are solved numerically with spectral methods⁵ and with impermeable boundaries at $r = R_1$ and R_2 . We use cylindrical, rather than the usual cartesian coordinates in equations (1) and (2) to allow a direct comparison with the cylindrical laboratory experiments of Sommeria *et al.*⁶.

I adopt the hypothesis that the jovian zone containing the Great Red Spot is an approximately axisymmetric, azimuthal flow with nearly uniform ω_p that contains isolated patches of non-uniformity (including the red spot). Although the hypothesis cannot be tested directly because $\bar{\psi}(r)$ and L_R are unknown, it is consistent with their known bounds¹. The motivation for this hypothesis is that numerical simulations have shown that fluids that obey equation (1) and that are mixed by external stirring tend to produce flows with nearly uniform ω_p over much of their domains^{7,8}. This evolution to homogeneous ω_p has also been observed in the laboratory⁶. Our numerical simulations of equations (1) and (2) in an annular geometry with no stirring also show that large regions with homogeneous ω_p form when the initial velocity is random but constrained so that its azimuthal average, $1/(2\pi) \int_0^{2\pi} v_\phi(r, \phi, t=0) d\phi$, is a linearly unstable solution of equation (1)⁹. (All axisymmetric, azimuthal flows are exact solutions of equation (1).)

Typically, the nearly axisymmetric, azimuthal flows with uniform ω_p produced in our simulations and in the experiments of Sommeria *et al.* contain a few, small, isolated vortices where the value of ω_p differs substantially from that of the surrounding azimuthal flow. Because the evolution of a general class of initial flows into nearly uniform ω_p flows containing isolated vortices is discussed elsewhere^{6,9}, each numerical simulation presented here begins with an exactly axisymmetric, azimuthal, uniform ω_p flow superposed with a finite number of spots of vorticity. We define $\tilde{v}_\phi(r, t)$ as the velocity of the uniform ω_p component of the flow, $\sigma = r\partial(\tilde{v}_\phi/r)/\partial r$ as its shear, and ω_e as the difference between the potential vorticity of a spot of vorticity and the ω_p of $\tilde{v}_\phi(r, t)$. Note that $\tilde{v}_\phi(r, t)$ is a neutrally stable solution of equation (1); it has no exponentially growing or decaying eigenmodes and cannot propagate Rossby waves⁹.

First, I show that spots with ω_e the same sign as σ are stable and those with opposite sign are pushed to the radial boundaries

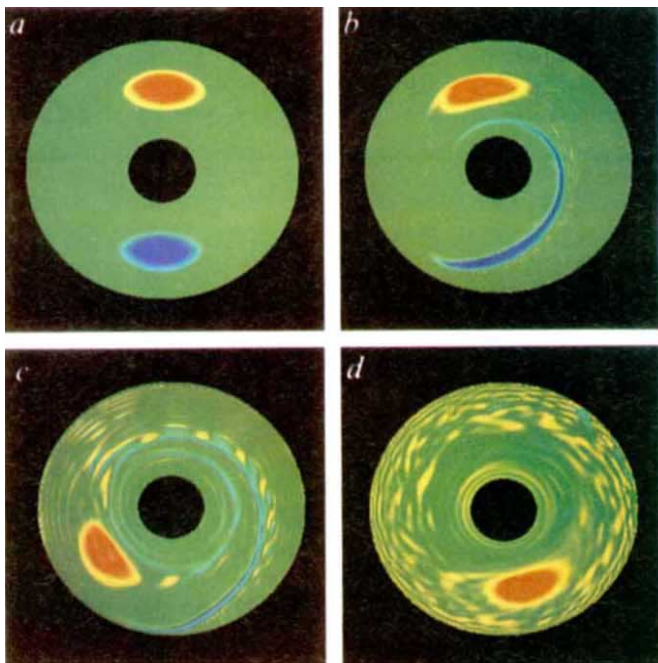


Fig. 1 The ω_e of two spots superposed with an axisymmetric, azimuthal, uniform ω_p flow with negative shear. The colour scale follows the order of the spectrum: $\omega_e < 0$ is red, $\omega_e = 0$ is green, and $\omega_e > 0$ is blue. The time is in units of the turn-around time of the initial spots (defined in the text). *a*, $t = 0.0$; *b*, $t = 0.50$; *c*, $t = 1.5$; *d*, $t = 4.8$.

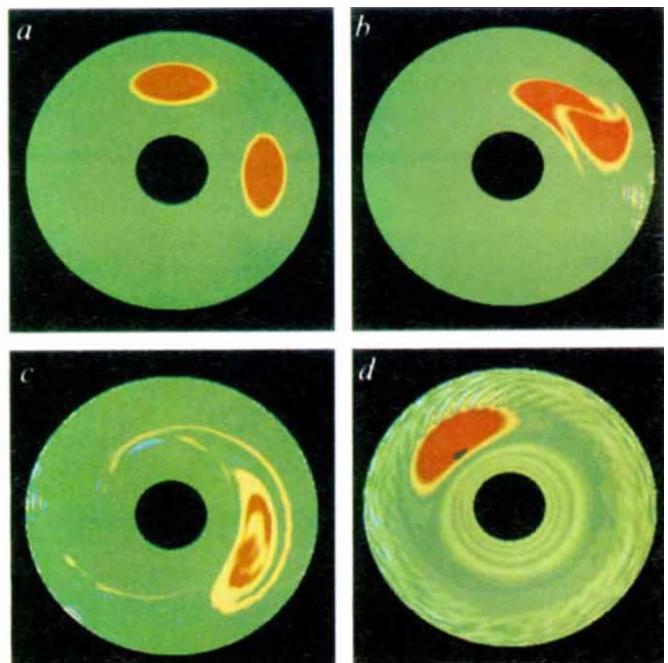


Fig. 2 Two stable spots initially superposed with an axisymmetric, azimuthal, uniform ω_p flow with negative shear. *a*, $t = 0.0$; *b*, $t = 1.3$; *c*, $t = 2.6$; *d*, $t = 28$.

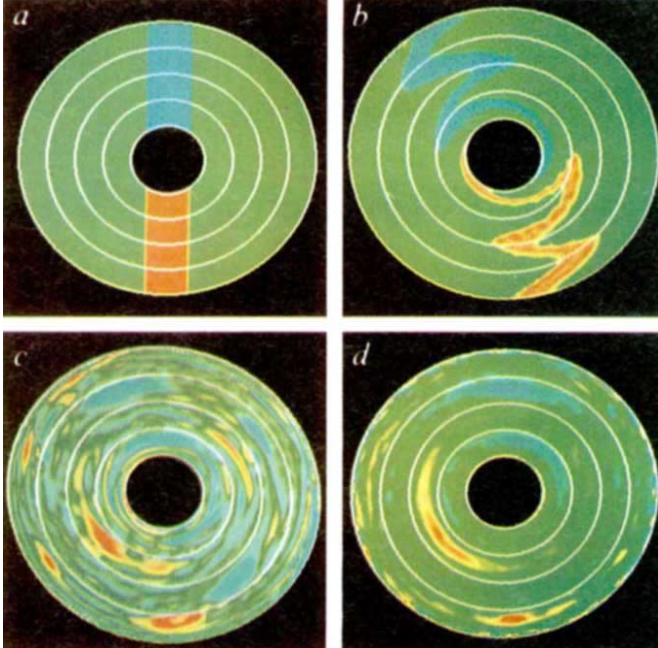


Fig. 3 Rectangular spots of positive and negative ω_e superposed initially with an axisymmetric, azimuthal, uniform ω_p flow with a sinusoidally varying shear. The white circles mark the radii where the shear changes sign. (These are also the extrema of the angular velocity of the azimuthal flow.) *a*, $t = 0.0$; *b*, $t = 0.057$; *c*, $t = 1.1$; *d*, $t = 11$.

of the azimuthal flow and fragment. Figure 1 shows a flow consisting initially of two spots of vorticity of equal strength and with approximately uniform ω_e but with opposite sign. The azimuthal flow superposed initially with the spots is $\tilde{v}_\phi(r, t = 0) = \beta r^2/3 + C/r$, where C is a constant equal to $\frac{1}{6}$. The flow has $\beta = 1$, $R_1 = 0.25$, $R_2 = 1.0$ and $L_R \rightarrow \infty$. The shear of the initial \tilde{v}_ϕ is $\sigma(r, t = 0) = \beta r/3 - 2C/r^2$, and is negative throughout the entire domain of the flow. Both spots have $|\omega_e| \approx 0.9$ (so $|\sigma/\omega_e| \approx 0.7$).

In Fig. 1*b* the red spot, with ω_e of the same sign as σ , is stable and becomes more elliptical, but the blue spot stretches into a spiral with its inner and outer edges pushed to the inner and outer boundaries, respectively. The spiral is Kelvin-Helmholtz unstable^{5,9}; it fragments and breaks apart (Fig. 1*c*). Finally, Fig. 1*d* shows an isolated red spot superposed on a chaotic (as determined by broad peaks in its power spectrum) azimuthal flow containing many small yellow and blue filaments. If the azimuthal flow is averaged over scales large compared to the

filaments but small compared with the red spot, it has uniform ω_p . The spot is advected with the velocity of the surrounding azimuthal flow. Although it continually loses and gains ω_e , it is statistically steady. The behaviour shown in Fig. 1 is representative for a wide range of values of the parameters β , ψ , L_R and C , including the case $\beta = \bar{\psi}(r) = 0$ (neither the gradient of the Coriolis force nor an underlying topography are essential), as long as $10 > |\sigma/\omega_e| > 0.1$ and $L_R \geq L_H$, where L_H is the characteristic length over which ω_e changes (not necessarily the same as the size of a spot—see below). When parameters are varied so that $|\omega_e/\sigma|$ or L_R decreases, the stable spots become more elongated in shape⁹. When $|\sigma/\omega_e| > 10$ they are so elongated that they can be Kelvin-Helmholtz unstable. When $|\sigma/\omega_e| < 0.1$ the spots behave as if there were no surrounding azimuthal flow present. Flows with $\sigma > 0$ have stable blue spots.

The merger of two stable spots is shown in Fig. 2. The flow parameters and the initial \tilde{v}_ϕ are the same as in Fig. 1, but both initial spots in Fig. 2a have $\omega_e < 0$. The spots are initially towards each other by the differential rotation of \tilde{v}_ϕ . As the spots approach, they distort, shed some ω_e (Fig. 2b), and merge, trapping weakly rotational fluid (yellow-coloured) at the vortex centre (Fig. 2c). The yellow streamer trailing from the vortex is Kelvin-Helmholtz unstable⁹ and becomes wavy. Figure 2d shows a statistically steady spot, superposed on a chaotic azimuthal flow. Yellow filaments torn from the spots make the azimuthal flow chaotic, but the azimuthal flow has uniform ω_p when averaged over length scales larger than the size of the filaments. The timescale for mergers is the turn-around time of a spot, $\tau \equiv 4\pi/\omega_e$. By varying the parameters and initial conditions, we have found that the size of the critical impact parameter (initial separation in r) necessary for two spots to merge increases approximately linearly with $|\sigma/\omega_e|$ and approximately equals the sum of the radial axes of the two merging spots. A derivation of the critical impact parameter based on the assumption that energy in the chaotic component of the flow is maximized was given earlier⁹. We have found circumstances where two spots do not merge if surrounded by a laminar azimuthal flow, but do merge if surrounded by a chaotic flow with small inhomogeneities in ω_p . A possible explanation is that the dynamics of two isolated spots is constrained to conserve energy and momentum. Small inhomogeneities in the azimuthal flow can exchange energy and momentum with the spots, relax the constraint, and thereby allow mergers.

Notice that between Fig. 2c and d the spot has expelled the weakly rotational, yellow fluid from its centre. We have never found a stable spot with a local minimum of ω_e at its centre. Flows that initially have \tilde{v}_ϕ superposed with many small spots, each with a different value of ω_e , can produce one large spot by mergers. Moreover, if the flow is so chaotic that the small spots are well-mixed with each other before and during the merging, the core of the large spot will have approximately uniform ω_e .

Figure 3 shows the dynamics of spots in a uniform ω_p flow where the shear of \tilde{v}_ϕ does not have a constant sign. Initially, $\sigma(r, t=0) = 3 \sin[4\pi(r-R_1)/(R_2-R_1)]/r$ and $\tilde{v}_\phi(r, t=0) = r \int_{R_1}^r \sigma(r', t=0)/r' dr' - 0.46r$. The parameters $\bar{\psi}(r)$ and L_R^2 were chosen such that $\bar{\psi}(r)/L_R^2 = \beta r - (1/r)(\partial/\partial r)[r\tilde{v}_\phi(r, t=0)]$ and $\psi(r, t)/L_R^2 \rightarrow 0$ (this limit corresponds to the ratio of the fluid density in the upper to lower layers approaching zero). The white circles show the radii where $\sigma = 0$. If we consider the annular regions between the circles as ‘zones’, then the σ of the four zones alternates in sign with the innermost zone having $\sigma > 0$. Initially, red and blue rectangular spots are superposed with \tilde{v}_ϕ , but these distort due to the differential rotation of \tilde{v}_ϕ (Fig. 3b). The distortion is at a maximum where \tilde{v}_ϕ/r has an extremum (at the white circles). The large spots quickly fragment, and pieces with ω_e of the opposite sign of the local $\sigma(r, t)$ are expelled from the zones (Fig. 3c). The small pieces of ω_e coalesce and form one large spot in each zone (Fig. 3d). The

spots alternate in colour from zone to zone and are highly elongated because $\sigma/\omega_e \approx 5$.

Figure 3 shows several properties common to all of our simulations: several zones with opposite shear can co-exist; stability of spots does not depend on the proximity of horizontal boundaries; the sign of the local σ determines which spots of ω_e are stable and which are ejected from a zone; spots grow by amalgamating other spots until they either overflow their own zone (see Fig. 3d) or have amalgamated all available ω_e (which occurs when the initial spots are smaller than those in Fig. 3a). Flows with spots that do not fill their entire zones tend to move to the radial location where $\sigma(r)$ have a local extremum, in agreement with the laboratory study of Sommeria *et al.*⁶ (An isolated spot can change its radial location only if it exchanges energy and momentum with another spot or with the small filaments of ω_e in the surrounding azimuthal flow.)

Although the dynamics of spots is similar throughout the range $L_R \geq L_H$, the vorticity and velocity distributions inside the spots vary qualitatively with the value of L_R : a uniform ω_e spot with finite L_R concentrates most of its vorticity at the edge of the spot and has a non-rotating centre. In contrast, a spot with uniform ω_e and with $L_R \rightarrow \infty$ has approximately uniform vorticity. This can be demonstrated analytically for the case $\beta = \sigma = \tilde{v}_\phi = 0$ where the spots are circular. The vorticity in a circular spot with $L_R \rightarrow \infty$ is exactly uniform, but with finite L_R , the vorticity is proportional to $I_0(\hat{r}/L_R)$, where \hat{r} is the distance from the centre of the spot and I_0 is a modified Bessel function that increases exponentially in \hat{r} . The vorticity drops abruptly by ω_e at the edge of the spot, and decreases exponentially (proportional to the Bessel function $K_0(\hat{r}/L_R)$) outside the spot.

The parameters of Jupiter's Great Red Spot, $\sigma/\omega_e \approx 1$ and $L_H/L_R \approx 1$, are within the range of values presented here, and the vorticity distribution and shape of the red spot agree qualitatively with our simulations. The dynamics of the red spot looks similar to our numerical simulations, especially the amalgamation of smaller spots, which often leaves trailing wisps of ω_e downstream of the red spot¹⁰. The red spot, like the flow in Fig. 3d, fills its zone (in the latitudinal direction) and like all of our simulated spots, does not drift with respect to \tilde{v}_ϕ except for the chaotic buffeting it gets from the small filaments embedded in \tilde{v}_ϕ .¹¹ (Note that the slow 90-day zonal oscillation of the red spot¹³ cannot be produced by our simulations.) There are other long-lived vortices on Jupiter with dynamics similar to the red spot¹¹ and our simulations. Although some rotate clockwise and others anti-clockwise, all of these spots rotate in the same direction as the local shear, which is consistent with our numerical simulations.

Because the velocity of the red spot increases exponentially outward (with $L_H \approx 2,200$ km) and has a non-rotating centre with most of its vorticity concentrated at its periphery, it is possible that it has uniform ω_e . This suggests that it was created by a chaotic amalgamation of smaller spots. To see if ω_e is uniform in the core of the red spot and to find the value of L_R at the spot, consider the variation of ω_e as a function of longitude (but at fixed latitude). Equivalently, consider the difference in ω_e between the points (r_c, ϕ) and (r_c, ϕ_c) where ϕ_c and r_c are the longitude and latitude (multiplied by the radius of Jupiter) of the centre of the spot. From equation (2) this difference is

$$\begin{aligned} \omega_e(r_c, \phi) - \omega_e(r_c, \phi_c) \\ = \omega(r_c, \phi) - \omega(r_c, \phi_c) - \frac{\psi(r_c, \phi) - \psi(r_c, \phi_c)}{L_R^2} \\ = \omega(r_c, \phi) - \omega(r_c, \phi_c) + \frac{r_c \int_{\phi_c}^{\phi} v_r(r_c, \phi') d\phi'}{L_R^2} \end{aligned} \quad (3)$$

where I have assumed that L_R is a function of r but not ϕ , and I have used $\psi(r_c, \phi) - \psi(r_c, \phi_c) = -r_c \int_{\phi_c}^{\phi} v_r(r_c, \phi') d\phi'$. The advantage of equation (3) over equation (2) is that it does not contain the unknown function $\psi(r)$. If the left-hand side of equation (3) is zero, the spot has uniform ω_e . Substituting the

observed values¹² of $v_r(r_c, \phi)$ and $\omega(r_c, \phi)$ into the right-hand side, we find that the left-hand side is ~ 0 when $L_R \approx 1,300$ km. The fit is particularly good for distances $< 9,000$ km from the centre of the red spot. (The semi-major axis of the red spot is $\sim 13,000$ km.) This calculation of L_R is the first to be made based on the dynamics of the red spot, and it is consistent with the estimates based on the thermal structure of the atmosphere³. This calculation suggests that the red spot has a large, 18,000-km diameter core with a nearly uniform potential vorticity, that the size of the spot is much greater than L_R , and that $L_R \approx L_H$.

The picture here is that the red spot is embedded in a chaotic but approximately uniform ω_p zone. It formed by amalgamating the small patches of ω_e that continually form on Jupiter due to small-scale processes (first suggested by Ingersoll¹¹), grew in size until it overflowed its zone, and is currently in statistical equilibrium—continually exchanging ω_e with the surrounding flow. Although my two-layer model of the jovian atmosphere is simplistic, it produces robust, long-lived vortices that are dynamically similar to the red spot. Future calculations will need to include a more realistic vertical structure. My assumption that the zone surrounding the red spot has a nearly uniform ω_p will also have to be tested. The spots of vorticity produced by our model are stable if they have the same sense of rotation as the zonal shear, can exist in chaotic flows, and tend to coalesce. The spots with finite L_R are like the jovian red spot in having

quiet interiors with vorticity mostly at their edges. The spots do not require the proximity of horizontal boundaries, nor finite values of β , L_R or $\bar{\psi}$ for stability. The values of these parameters do not strongly influence the dynamics of spots, but they do determine the sign and strength of $\tilde{v}_\phi(r, t)$ and the vorticity distribution and shape of spots.

I thank H. L. Swinney and J. Sommeria for discussions and insight and B. Scott for the colour figures. The work was sponsored by NSF, the Office of Naval Research and the Lawrence Livermore National Laboratory.

Received 25 June; accepted 11 December 1987.

1. Ingersoll, A. P. & Cuong, P. G. *J. atmos. Sci.* **38**, 2067–2076 (1981).
2. Pedlosky, J. *Geophysical Fluid Dynamics* (Springer, New York, 1979).
3. Conrath, B. J., Flasar, F. M., Pirraglia, J. A., Gierasch, P. J., Hunt, G. E. *J. geophys. Res.* **86**, 8769–8775 (1981).
4. Limaye, S. S. *Icarus* **65**, 335–352 (1986).
5. Marcus, P. S. in *Numerical Analysis* (eds Griffiths, D. F. & Watson, G. A.) 125–139 (Longman Scientific and Technical, Harlow, 1986).
6. Sommeria, J., Meyers, S. D., Swinney, H. L. *Nature* **331**, 689–693 (1988).
7. Rhines, P. B. & Young, W. R. *J. Fluid Mech.* **122**, 347–367 (1982).
8. Williams, G. P. *J. atmos. Sci.* **36**, 932–968 (1979).
9. Marcus, P. S. *J. Fluid Mech.* (submitted).
10. Low, M.-M., M. & Ingersoll, A. P. *Icarus* **65**, 353–369 (1986).
11. Beebe, R. F. & Hockey, T. A. *Icarus* **67**, 96–105 (1986).
12. Mitchell, J. L., Beebe, R. F., Ingersoll, A. P. & Garneau, G. W. *J. geophys. Res.* **86**, 8751–8757 (1981).
13. Smith, B. A. & Hunt, G. E. in *Jupiter* (ed. Gehrels, T.) 564–585 (University of Arizona Press, Tucson, 1976).

Direct identification of superconducting regions in an inhomogeneous specimen by electron shadow microscopy

Yang Cui-Ying & J. W. Steeds

Physics Department, University of Bristol, Bristol BS8 1TL, UK

Scanning and transmission electron microscopy have played a major part in evaluating the microstructure of the new high-temperature superconductors. Complex fabrication routes have led to a wide variety of phases in the samples produced, and the high-temperature superconductor itself has a complex microstructure on which its superconducting properties are dependent. Finally, the process of preparing specimens for examination by electron microscopy can itself lead to degradation of the superconducting properties. As a result it is desirable to establish directly that the regions studied are indeed superconducting, and to relate the superconducting properties to the local microstructure. Here we describe a convenient method for performing such an evaluation. One possible method, which relies on image contrast in a scanning electron microscope, was recently proposed¹. Another, which we discuss here, involves the use of a long established, if little used, technique of electron shadow microscopy².

The technique is closely related to Schlieren microscopy. Flux exclusion from superconducting regions leads to local changes in the magnetic field which cause Lorentz deflection of the high-energy electrons in a transmission electron microscope. The focusing effects of the complicated form of the resultant magnetic fields give rise to the well-known classes of catastrophes in optics which are now well-understood³. In the simplest case, cycloidal shadows are produced⁴, and numerical calculations of the shadow patterns produced by superconducting lead cylinder were performed⁵.

In order to pursue these experiments, we decided to abandon the fracture chip method of specimen preparation mostly used in previous transmission electron microscopy experiments on the new superconductors. Our main aim was to relate microscopic observations to macroscopic specimens, and for this purpose we decided to ion-thin sections of the material prepared. On fracturing, the location of a fragment in the original specimen

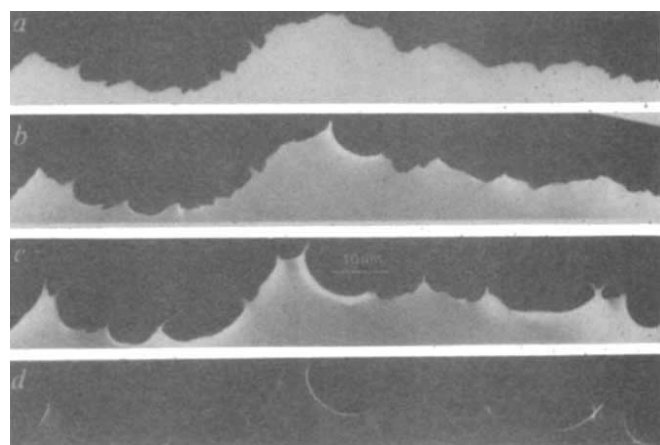


Fig. 1 Shadow image of the edge of an ion-thinned sample at the approximate temperatures *a*, 90 K; *b*, 74 K; *c*, 35 K; *d*, 35 K. Short exposure was employed to reveal details of the caustic figures.

is lost; moreover the technique is generally selective and fails to pick out all the components of a multiphase preparation. However, ion-thinning of samples is known to introduce damage⁶ and considerable care had to be exercised in obtaining satisfactory samples.

It was also important to have a double-tilting liquid helium cooled specimen holder available for the experiments reported here. Even though the superconducting transition temperature of $\text{YBa}_2\text{Cu}_3\text{O}_x$ is well above that of liquid nitrogen, it is unlikely that fracture chips reach this temperature in liquid nitrogen cooled holders. Cooling by conduction via the tortuous path required to reach the fracture chip is unlikely to be very effective. In addition, the thin specimens, with aspect ratios which are typically not less than 100:1, were mounted perpendicular to a magnetic field of ~ 1.5 T. The resulting demagnetizing fields will have caused flux penetration into the sample.

Some initial work was performed with fracture chip specimens to identify unambiguously the $\text{YBa}_2\text{Cu}_3\text{O}_x$ phase in our preparations (see, for example, refs 7 and 8). After a while it was possible to pick these out by their twinned microstructure,